

Printed: October 27, 2018

Disentangling the Nature of the Radio Emission in Wolf Rayet Stars

Gabriela Montes^{1,2}, Miguel A. Pérez-Torres¹, Antonio Alberdi¹, and Ricardo F. González²

ABSTRACT

We present quasi-simultaneous, multi-frequency VLA observations at 4.8, 8.4, and 22.5 GHz, of a sample of 13 Wolf Rayet (WR) stars, aimed at disentangling the nature of their radio emission and the possible detection of a non-thermal behavior in close binary systems. We detected 12 stars from our sample, for which we derived spectral information and estimated their mass loss rates. From our data, we identified four thermal sources (WR 89, 113, 138, and 141), and three sources with a composite spectrum (similar contribution of thermal and non-thermal emission; WR 8, 98, and 156). On the other hand, from the comparison with previous observations, we confirm the non-thermal spectrum of one (WR 105), and also found evidence of a composite spectrum for WR 79a, 98a, 104, and 133. Finally, we discuss the possible scenarios to explain the nature of the emission for the observed objects.

Subject headings: radio continuum: stars - stars: Wolf-Rayet, - binaries: close - stars: individual (WR 98, WR 133, WR 156)

1. INTRODUCTION

Wolf Rayet (WR) stars are evolved, massive stars that are losing their mass rapidly through strong stellar winds (Conti 1976). In this scenario, hot, massive OB stars are considered to be the WR precursors that lose their external layers via stellar winds, leaving exposed their He-burning nuclei and H-rich surfaces. The stellar winds of WR stars display

¹Instituto de Astrofísica de Andalucía, (IAA-CSIC), Camino Bajo de Huétor 50, E-18008 Granada, Spain; gmontes@iaa.es, torres@iaa.es, antxon@iaa.es

²Centro de Radioastronomía y Astrofísica UNAM, Apartado Postal 3-72 (Xangari), 58089 Morelia, Michoacán, México; g.montes@astrosmo.unam.mx, rf.gonzalez@astrosmo.unam.mx

high mass-loss rates [$\dot{M} \approx (2-5) \times 10^{-5} M_{\odot} \text{ yr}^{-1}$] (e.g. Abbott et al. 1986, hereafter AB86; Crowther et al. 1995; Leitherer et al. 1995, 1997, hereafter LC95, LC97) and high terminal velocities [$v \approx (1000 - 2000) \text{ km s}^{-1}$] (e.g. Crowther et al. 1995). These stellar winds reveal themselves at several frequency ranges, e.g., tracing the terminal velocity in the P Cygni profiles in UV (Crowther et al. 1995), or showing an excess of emission at IR and radio frequencies (e.g. AB86, Contreras et al. 2004).

At radio frequencies, the excess of emission is associated with the contribution of the free-free thermal emission coming from the ionized and expanding envelope formed by the stellar wind. Early studies by Panagia & Felli (1975; hereafter PF75), and Wright & Barlow (1975; hereafter WB95) found that the thermal radio emission of an ionized, spherically symmetric, steady wind with an electron density profile, $n_e \propto r^{-2}$ (r being the distance from the central star), follows a power-law with frequency, $S_{\nu} \propto \nu^{\alpha}$, with a positive spectral index $\alpha \approx 0.6$ (hereafter this stellar wind is referred to as “standard” wind). These authors also derived simple, useful relations between observable quantities, the flux density S_{ν} and the mass-loss rate \dot{M} of the star. On the other hand, negative and flat ($\alpha \sim 0$) spectral indices are also observed in massive stars. These spectral indices are thought to be an indication of a composite spectrum, with a thermal plus a non-thermal contribution. The non-thermal emission is thought to be synchrotron emission produced by relativistic electrons, which have been accelerated either in strong shocks within the stellar wind, for single stars (White 1985), or in a wind-collision region (WCR) between the stellar components for binary systems (WR+0; Usov 1992, Eichler & Usov 1993). Therefore, radio observations can determine both \dot{M} and, through simultaneous multi-frequency observations, the spectral index α , which characterizes the emission process.

In this way, observations can allow to identify the presence of both thermal, and non-thermal emission in WR stars (AB86, LC95, LC97, Chapman et al. 1999, Contreras et al. 2004, Cappa et al. 2004). For thermal sources, deviations from a standard wind, could result in the spectral index being either steeper (>0.6 ; Nugis et al. 1998) or slightly flatter than 0.6 (WB95). On the other hand, for non-thermal sources it is unclear whether the conditions to produce synchrotron emission are present in all of these stars. Recently, theoretical (Van Loo 2005) and observational (Dougherty & Williams 2000, hereafter DW00) studies suggest that non-thermal sources require a binary companion. For the synchrotron emission to be detected, this must be produced within the optically-thin region of both stellar winds (Pittard et al. 2006), or there must be some low-opacity lines-of-sight in the wind through which we are observing the emission (DW00). For wide binary systems ($P > 1 \text{ yr}$), the non-thermal detection of the WCR has been supported by theoretical (Dougherty et al. 2003, Pittard et al. 2006) and observational studies (e.g. WR 147, Williams et al. 1997; WR 140, Dougherty et al. 2005). However, for close ($P < 1 \text{ yr}$) binary systems, it is unlikely that the

emission from the WCR could be detected, since it is expected to be absorbed by the dense WR stellar wind (DW00).

In this paper, we present simultaneous, multi-frequency observations of a sample of 13 WR stars, using the VLA at 4.8, 8.4, and 22.5 GHz, aimed at disentangling the origin of their stellar wind radio emission through the analysis of their spectral index and time variability by comparison with previous observations. In particular, we focus on the possible detection of the WCR emission in close binary systems, and present new observations of two single stars previously classified as non-thermal sources. In Section 2, we describe our observations. In Section 3, we show our results, classification of emission nature, and mass-loss rate, \dot{M} , determinations for each of the stars detected in our sample. We discuss our results in Section 4, describing common scenarios for the sources with similar spectrum behavior. Finally in Section 5 we summarize of our main results.

2. OBSERVATIONS

We performed radio observations of a sample of 13 WR stars, listed in Table 1, with the Very Large Array (VLA) of the National Radio Astronomy Observatory (NRAO)¹. Two sets of observations were performed in 2007 while the VLA was in D configuration: we observed five sources on April 21 at 4.8 and 8.4 GHz, and three additional sources on May 6 at 4.8, 8.4, and 22.5 GHz. In March 2008, we observed seven sources with the VLA in C configuration: five of them were new sources and the other two were also observed in 2007 (WR 79a and WR 105).

Data editing and calibration were carried out using the NRAO Astronomical Image Processing System (AIPS) package, following standard VLA procedures. Absolute flux calibration was achieved by observing 3C 48 and 3C 286. The phase calibrators used for each observation and their flux densities at each of the observing frequencies, as well as the uncertainties from the calibration, are given in Table 2. For WR 105, self-calibration at 22.5 GHz allowed us to improve the phase calibration of this source. However, for the rest of the sources self-calibration was not possible because of the weakness of the sources. Expected off-source rms of ~ 50 and $\sim 40\mu\text{Jy}/\text{beam}$ at 4.8 and 8.4 GHz respectively, and $\sim 60\mu\text{Jy}/\text{beam}$ at 23 GHz, were successfully achieved for most of the sources, with an on-source time of 15 minutes at 4.8 and 8.4 GHz, and of 30 minutes at 22.5 GHz. However, the observations of WR 79a, 89, 104, and 105, which were obtained with the VLA in D configuration, suffered

¹The NRAO is a facility of the National Science Foundation operated under cooperative agreement by Associated Universities, Inc.

from sidelobe contamination, resulting in an increase of the rms noise. We improved the rms of those images by excluding the short baselines in the AIPS-IMAGR (UVRANGE=3,0). We used the AIPS-IMFIT procedure in order to fit the position and flux density of the detected sources. Since the sources are not expected to be resolved, we fixed in IMFIT the standard parameters for unresolved sources. We took a box size approximately twice the beam size of each image. This procedure fits a 2D-Gaussian to the sources and estimates the position of the maximum, the total flux density, and the errors of these determinations. The error estimated by IMFIT considers both the quality of the fit and the image rms.

We present in Table 3 the position, total flux density, and spectral indices obtained for the 12 detected sources. The flux density uncertainties were calculated considering both the IMFIT error estimates and 2% calibration uncertainties at 4.8 and 8.4 GHz, and 5% at 22.5 GHz. Note that the rms noise of the image is the dominant contribution to the error budget. The upper limits of the undetected sources were taken as three times the rms noise.

We also used unreported archival VLA data for WR 105 and WR 133, searching for a possible variability in their radio emission which would indicate a likely non-thermal origin. For WR 105 we used VLA observations in B configuration taken on November 20, 1999 at 1.4, 4.8, and 8.4 GHz, and on November 27, 1999 at 4.8, 8.4 and 15 GHz. For WR 133, we analyzed observations on May 31, 1993 at 1.4, 4.8, and 8.4 GHz, when the VLA was in BC configuration. We should note that the VLA configuration was not relevant for our purpose, since we were interested only in the flux density of the stars, which are not resolved at any VLA configuration. We calibrated these archival data in a similar way than our observations, reaching similar values for the rms noise. For WR 105, self-calibration could be performed at all the observed frequencies.

3. RESULTS

3.1. Spectral Index Determinations

We observed a total of 13 WR stars and detected 12 of them at least at one frequency. In Table 3 we present the flux densities of the detected sources at each observed frequency, as well as upper limits for the undetected sources. All the sources were observed quasi-simultaneously at different frequencies on the same day, six of them observed in this way for the first time (WR 8, 98, 113, 138, 141 and 156). Owing to the observed flux density variability for this kind of sources, we point out the importance of the simultaneity in order to correctly determine their spectral index. Using this approach, we derived spectral indices for the eight sources detected at all observing frequencies. We also derived lower limits for

the spectral indices of the remaining four sources that were detected at least at one frequency, but with only an upper limit for the flux density at another. When only two frequencies were available, the spectral index was determined using the logarithmic ratio of the flux densities and the observing frequencies. Otherwise, when three frequencies were available, we used a linear regression fit weighting each data point by its error. For WR 133 we have not used the data at the lower frequencies to determine its spectral index. The archival data at 1.4 GHz had a large rms noise, which prevented us from fixing a reliable upper limit for its flux density. On the other hand, our 4.8 GHz data did not allow us to determine an upper limit to the flux density, since WR 133 is diluted by the unresolved emission of a source to the northeast of the WR 133 position.

3.2. Disentangling the Nature of the Emission

The thermal stellar winds are expected to have spectral indices ~ 0.6 (WB75, Nugis et al. 1998). On the other hand, in non-thermal WR stars, the contribution of the thermal emission from the stellar winds combined with a non-thermal component from the WCR, will result in a total spectrum characterized by spectral indices < 0.6 (e.g. Eichler & Usov 1993). This non-thermal emission is expected to be modulated by the orbital motion of the system, resulting into variability of the total spectrum (e.g. WR 140; Dougherty et al. 2005) with a periodicity related with the orbital period.

In order to classify the nature of the WR radio emission, we have determined i) the spectral index for each source and observing epoch and ii) the presence of variability by comparing all the flux density measurements from the different observing epochs. We considered the existence of flux density variability when the differences in the flux densities between two or more epochs are higher than 3σ . For the spectral index, we use a conservative 3σ criterion as a significant difference. Optically-thin thermal emission (for which $\alpha \sim -0.1$) is not expected for these massive stars at these frequencies (DW00). In this way, we classified our sources as follows:

- Thermal (T; free-free thermal emission): sources with a spectral index $\gtrsim 0.6$ for all the observing epochs.
- Non-thermal (NT; dominant non-thermal emission): sources that showed a spectral index $\lesssim -0.1$ for at least one observing epoch, as well as variability in their emission.
- Composite (T/NT; thermal+non-thermal): sources that presented spectral indices higher than -0.1 but flatter than 0.6 (for at least one observing epoch), as well as variability in their emission.

Applying these criteria to the spectral indices and flux densities determined from these and previous observations, we found that at least four sources are T (WR 89, 113, 138, and 141), one is NT (WR 105), and three present a T/NT behavior (WR 8, WR 79a, and 156).

For the rest of the sources we have relaxed those criteria (WR 98, 98a, 104, and 133), since their strict application would mask important characteristics of these sources. For WR 98a and WR 104, we have also considered the modeling of the emission presented by Monnier et al. (2002), and classified them as T/NT sources. For WR 98, the first determination of the spectral index is not conclusive about its spectrum; therefore, we also have taken into account the short time variability (15 days, see Table 4) at 4.8 GHz as a plausible indication of a possible non-thermal emission and a tentative T/NT nature. For WR 133, it is difficult to infer a variability in the spectrum from the two spectral index determinations, since those were determined from different frequency ranges (see Table 4). However, we should point out that the lower frequency range of WR 133 shows a tendency towards a non-thermal spectrum in the 1993 epoch. Therefore, we classified WR 98 and WR 133 as tentative T/NT sources.

Summarizing, we have found four T (WR 89, 113, 138, and 141), one NT (WR 105), and seven T/NT sources (WR 8, 79a, 98, 98a, 104, 133, and 156).

3.3. Mass-Loss Rates

As we mentioned in Section 1, it is possible to estimate the free-free radiation emitted from ionized extended envelopes. PF75 and WB75 assumed a “standard wind” (steady and completely ionized, with electron density profile $n_e \propto r^{-2}$, and expansion velocity v_∞), and showed that its flux density at radio frequencies follows a power law with frequency as $S_\nu \propto \nu^{0.6}$. Furthermore, those authors derived a general expression for the mass-loss rate, \dot{M} , in terms of observable quantities,

$$\left[\frac{\dot{M}}{M_\odot \text{ yr}^{-1}} \right] = 5.34 \times 10^{-4} \left[\frac{S_\nu}{\text{mJy}} \right]^{3/4} \left[\frac{v_\infty}{\text{km s}^{-1}} \right] \left[\frac{d}{\text{kpc}} \right]^{3/2} \left[\frac{\nu}{\text{Hz}} \right]^{-1/2} \left[\frac{\mu^2}{Z\gamma g_\nu} \right]^{1/2}, \quad (1)$$

where v_∞ is the terminal velocity of the stellar wind, d is the distance to the star, ν is the observed frequency, and g_ν is the free-free Gaunt factor. The parameters μ , Z and γ are the mean molecular weight, the average ionic charge, and the mean number of electrons per ion, respectively.

In Table 5, we present \dot{M} determination using equation (1) for the 12 sources of our sample detected at 8.4 GHz. Those determinations were done by assuming a standard stellar

wind with a filling factor, $f = 1$; however, deviations from such assumptions might lead into an overestimation of \dot{M} .

For the sources identified as NT and T/NT, the additional contribution to the thermal stellar wind emission would cause an overestimation for the \dot{M} values. On the other hand, for the T sources, although their spectral indices higher than 0.6 suggest an overestimation for \dot{M} , their impact is not expected to be significant at this frequency (Montes et al. in preparation). Therefore, these determinations can be considered reliable, at least for the T sources.

The values μ , Z , and γ were taken from CG04. For WR 138 and WR 141 we adopted the values of WR 133, since they share the same spectral type, WN5. We compute g_ν from equation (3) within Leitherer & Robert (1991), adopting $T_e = 10^4$ K (deviations from this temperature have minor effects on g_ν). The terminal velocities v_∞ and distances d of the stars were obtained from the van der Hucht (2001) WR catalog. We estimated the uncertainties for each parameter in Table 5 using the same criteria as in LC97. For the parameter d we assumed a 20% error based on the cluster/association membership of the star, otherwise 40% errors are assumed (0.09 and 0.25 dex, respectively). For the errors in v_∞ we assume 10% (0.04 dex). The error obtained in g_ν is about 10%. Finally, for μ , Z , and γ we assumed an error of ± 0.08 dex, as in CG04. Therefore, following the equation (5) in LC97 for the \dot{M} uncertainties, we obtained a typical logarithmic error of 0.21 for the stars considered in cluster/association and 0.41 for the rest (WR 98, 98a, 104, and 156).

We compared our results for \dot{M} with those previously reported by Cappa et al. (2004), we calculated the average \dot{M} for each of the main spectral types in the sample, $\dot{M}(\text{WN}) = (3.05 \pm 2.21) \times 10^{-5} \text{ M}_\odot \text{ yr}^{-1}$ and $\dot{M}(\text{WC}) = (3.07 \pm 2.73) \times 10^{-5} \text{ M}_\odot \text{ yr}^{-1}$, for WN and WC respectively. We compared and found these values to coincide within the errors with those presented by Cappa et al. (2004; $\dot{M}(\text{WN}) \sim 4 \times 10^{-5} \text{ M}_\odot \text{ yr}^{-1}$ and $\dot{M}(\text{WC}8-9) \sim 2 \times 10^{-5} \text{ M}_\odot \text{ yr}^{-1}$). Nevertheless, this coincidence must be taken carefully due to the expected overestimation of \dot{M} mentioned above.

4. DISCUSSION

The results of our observations presented in Section 3 provide relevant information about the nature of the radio emission of the 12 detected WR stars. The detected flux densities and spectral indices displayed by the sources of our sample indicate the existence of thermal, non-thermal dominant, and composite spectrum sources.

For the sources identified as thermal (WR 89, 113, 138, and 141), we found spectral

indices ~ 1 . In a single star context, when the radio-continuum spectrum is consistent with thermal emission, the deviations of the expected 0.6 value for an isotropic wind (PF75 and WB75) may be caused either by the presence of condensations (clumps) that produce non-standard electron density profile ($n \propto r^{-s}$; with $s \neq 2$), or by internal shocks which result from variations in the wind parameters at injection (see González & Cantó 2008). Specifically, spectral indices higher than 0.6, may be the result of density profiles that fall off more rapidly than $n \propto r^{-2}$. On the other hand, for close binary systems, although the non-thermal emission from the WCR is expected to be absorbed by the WR stellar wind, the hot and dense shocked gas within the WCR might be able to contribute to the thermal radio spectrum (Stevens et al. 1995, Pittard et al. 2006, Pittard 2009). Moreover, in these kind of systems, it is possible that the WCR turns radiative, resulting in a dense and optically-thick thermal emitting structure with a positive spectral index ($\gtrsim 1$) (Pittard 2009, Montes et al. in preparation). The nature of the WCR can be quantified through the ratio of the cooling time-scale for the shocked gas to the dynamical time-scale for it to flow out of the system $\chi \approx v_8^4 D_{12} / \dot{M}_{-7}$, where v_8 is the pre-shock velocity in units of 10^8 cm s^{-1} , D_{12} is the stellar separation in units of 10^{12} cm , and \dot{M}_{-7} is the stellar mass-loss rate in units of $10^{-7} \text{ M}_{\odot} \text{ yr}^{-1}$ (Stevens et al. 1992). In this way, the WCR can be either radiative ($\chi < 1$) or adiabatic ($\chi \gtrsim 1$). For the binary thermal sources in our sample, $D < 1 \text{ AU}$ which implies $\chi < 0.5$, according to the stellar wind parameters given in Table 5. This suggests a radiative WCR with a thermal contribution to the spectrum, which might be able to turn its spectral index into such positive values. Therefore, for WR 113, 138 and 141, although their high spectral indices (~ 1) might result from a clumpy single stellar wind, it is also possible that such spectral indices are also indicating a binary star system. Moreover, for WR 141 there seems to be evidence for the presence of a WCR region from observations at other frequencies (X-rays, Oskinova 2005, and spectral analysis, Moffat et al. 1996).

On the other hand, the non-thermal indications of the single stars WR 79a (T/NT) and WR 105 (NT) have no clear explanation. A non-thermal component in WR stars seem to be closely related to the binary nature of the star. DW00 analyzed the radio emission of a sample of 23 WR stars. They found that most of the sources with a non-thermal signature were binary systems, which suggests that binarity is intrinsically related to the detection of non-thermal emission. In this scenario non-thermal emission is thought to be produced within a WCR between the two stellar components. However, WR 79a and WR 105 do not show any evidence of binarity (Marchenko et al 1998). Van Loo et al. (2006) presented a study of the non-thermal emission produced by wind-embedded shocks resulting from instabilities within a single O-type stellar wind (also applicable to WR stars). They found that the radial decline of the shock strength (velocity jump and compression ratio) produces a rapid decrease of the synchrotron emission, becoming negligible at those radii where the

stellar wind becomes optically-thin. This rules out the detection of a non-thermal component in a single star. Moreover, as pointed out by DW00, proving that a star is single is very difficult, and we cannot rule out the presence of a companion in these stars. Since detectable non-thermal emission depends, in part, on the binary separation and the inclination angle of the system (e.g. WR 140 Dougherty et al. 2005), the detected flux density is expected to be modulated by the orbital motion, showing variability with a periodic behavior. Therefore, the observed variability in the spectra of WR 79a and WR 105 might be an indication of binary systems. Observations of WR 105 show variability in its 4.8 GHz flux density over a period of time of ~ 14 yr. For WR 79a the emission at 8.4 GHz increases $\sim 50\%$ between 2001 and 2005 observations (see Table 4). However, shorter variability time-scales in those sources can not be ruled out, as observations do not allow for a precise determination of their variability time scale and orbital period.

The tentative T/NT sources WR 98 and WR 133, are close binaries with periods of 47.8 and 112.4 days, respectively. Assuming a total mass for the system $M = 50 M_{\odot}$, the semi-major axis of the orbits are ~ 1 AU and 1.7 AU, respectively. Non-thermal emission arising from a WCR in these systems must be within the optically-thick region of the WR stellar wind ($\gtrsim 30$ AU at 4.8 GHz; from equation (25) in PF75) and then not detectable. This seems difficult to reconcile with the tentative T/NT behavior displayed by WR 98 and WR 133. In fact, the short periods of these systems make it unlikely that the separation between the components (D) increases (even for a high eccentricity), at least to those radii required for non-thermal emission to escape the absorption (~ 30 AU). Pittard et al. (2006) analyzed the thermal emission arising from non-radiative WCR (according to Stevens et al. 1992), and pointed out that thermal emission from the WCR may increase when D decreases (see Figure 11 in Pittard et al. 2006), contributing significantly to the total thermal flux, and resulting in a spectrum that may mimic a non-thermal contribution. In this scenario, an enhancement of 40% in the flux density (at 4.8 GHz) of the system WR 98 would suggest a decrease of 29% in the separation D (since the thermal emission from the WCR is expected to scale as D^{-1}). However, a WCR within this system would be roughly isothermal ($\chi \sim 0.1$) with a positive thermal spectrum (Montes et al. in preparation). Therefore the tentative T/NT behavior for WR 98 is likely to be non-thermal emission from the WCR that is able to escape the absorption at certain orbital phases. On the other hand, for WR 133 the WCR is likely to be adiabatic ($\chi \gtrsim 1$) with a flat thermal spectrum (see Pittard et al. 2006). For WR 133 the presence of WCR is also supported by the strong emission at X-ray energies (Oskinova 2005) and optical spectroscopic analysis (Underhill & Hill, 1994). However its influence at radio frequencies remains unclear, since the high errors of the spectral indices and the lack of observing epochs do not allow to infer any variability. Detailed theoretical models are required to determine whether a spectrum like T/NT can be reproduced entirely

by thermal emission or the non-thermal emission is able to be detectable for these systems.

WR 98a and WR 104 are well known colliding-wind binaries with an expanding dust spiral, called ‘pinwheel nebulae’ (Tuthill et al. 1999, Monnier et al. 1999, Tuthill et al. 2008). Monnier et al. (2002) modeled their radio emission taking into account a thermal plus an absorbed non-thermal component. At 8.4 GHz, we detected WR 98a, but only marginally WR 104. However, we have not detected either of these sources at 4.8 GHz, probably as a consequence of the strong absorption of the non-thermal emission described by Monnier et al. (2002). This absorption, and the lack of information about the flux density at higher frequencies, are likely to be the reason for the high value of the lower limits for their spectral indices.

Finally, although we classified WR 8 and WR 156 as T/NT, we can not completely rule out a single thermal wind origin of the observed emission. The binarity of WR 8 have been questioned by Crowther et al. (1995). Moreover emission variability was only marginally determined from our criterion, and the uncertainty of its spectral index is high. The same occurs for the flux density and spectral index determinations of WR 156. Further radio observations of both stars are needed to confirm its emission nature.

5. SUMMARY

We have presented simultaneous, multi-frequency observations of 13 WR stars at 4.8, 8.4, and 23 GHz. We have detected 12 of the observed sources at least at one frequency. The simultaneity of our observations have allowed us to obtain a reliable spectral index determination. In this way, we have determined spectral indices for eight, and lower limits for four of our 12 detected sources, being for six of them the first determinations. From the observed flux densities, spectral index determinations, and the comparison of our results with previous ones, we have disentangled the nature of the emission in these WR stars. We have also presented \dot{M} determinations, using our 8.4 GHz VLA flux density measurements. Those mass-loss rate estimates are consistent with values previously determined for WR stars.

We have classified WR 89, 113, 138, and 141 as thermal sources, for which $\alpha > 0.6$. We suggest different scenarios to reproduce the observed values for the spectral index. Such scenarios are mainly characterized by deviations from the standard wind, such as a different dependence with r for the electron density profile ($s \neq 2$), variability of both \dot{M} and v_∞ , and/or the influence of a binary companion.

WR 105, is likely a NT source owing to their significant flux density variability and the

negative spectral index for at least one observing epoch. WR 8, 79a, 98, 98a, 104, 133, and 156 show indications for a composite spectrum (T/NT).

The origin of the non-thermal signature for some of the sources of our sample is not completely clear, neither in the single stars (WR 79 and WR 105), nor in the close binary systems (WR 8, 98, and 133). The non-thermal signature in the WR 79a and WR 105 spectrum (thought to be single stars), could be explained by the presence of an undetected companion star. We also note the importance of carrying out a radio monitoring of the close binary systems WR 98 and WR 133. In fact, in case the flux density variability had a periodic behavior in those systems, and the period would happen to coincide with their orbital periods, this would unambiguously point to a binary origin of their NT signature.

Acknowledgements. We thank an anonymous referee for useful comments. GM acknowledges financial support from CSIC predoctoral I3P and JAE fellowship. MAPT research is funded through a Ramon & Cajal Fellowship of the Spain Ministry of Science (MEC) and the Spanish Research Council (CSIC). GM, MAPT and AA acknowledge support from the Spanish MEC through grant AYA 2006-14986-C02-01, and from the Consejería de Innovación, Ciencia y Empresa of Junta de Andalucía through grants FQM-1747 and TIC-126.

REFERENCES

- Abbott, D. C., Torres, A. V., Biegging, J. H., & Churchwell, E. 1986, *ApJ*, 303, 239
- Annuik, K. 1990, *Acta Astronomica*, 40, 267
- Bohannan, B., & Crowther, P. A. 1999, *ApJ*, 511, 374
- Biegging, J. H., Abbott, D. C., & Churchwell, E. B. 1982, *ApJ*, 263, 207
- Biegging, J. H., Abbott, D. C., & Churchwell, E. B. 1989, *ApJ*, 340, 518
- Cappa, C., Goss, W. M., & van der Hucht, K. A. 2004, *AJ*, 127, 2885
- Chapman, J. M., Leitherer, C., Koribalski, B., Bouter, R., & Storey, M. 1999, *ApJ*, 518, 890
- Cranmer, S. R., & Owocki, S. P. 1994, *Bulletin of the American Astronomical Society*, 26, 1446
- Conti, P. S. 1976, *Memoires of the Societe Royale des Sciences de Liege*, 9, 193
- Contreras, M. E., Montes, G., & Wilkin, F. P. 2004, *Revista Mexicana de Astronomia y Astrofisica*, 40, 53
- Crowther, P. A., Smith, L. J., & Willis, A. J. 1995, *A&A*, 304, 269
- Dougherty, S. M., & Williams, P. M. 2000, *MNRAS*, 319, 1005

- Dougherty, S. M., Pittard, J. M., Kasian, L., Coker, R. F., Williams, P. M., & Lloyd, H. M. 2003, *A&A*, 409, 217
- Dougherty, S. M., Beasley, A. J., Claussen, M. J., Zauderer, B. A., & Bolingbroke, N. J. 2005, *ApJ*, 623, 447
- Eichler, D., & Usov, V. 1993, *ApJ*, 402, 271
- Gamen, R. C., & Niemela, V. S. 2002, *New Astronomy*, 7, 511
- González, R. F., & Cantó, J. 2008, *A&A*, 477, 373
- Hamann, W.-R., Gräfener, G., & Liermann, A. 2006, *A&A*, 457, 1015
- Leitherer, C., & Robert, C. 1991, *ApJ*, 377, 629
- Leitherer, C., Chapman, J. M., & Koribalski, B. 1995, *ApJ*, 450, 289
- Leitherer, C., Chapman, J. M., & Koribalski, B. 1997, *ApJ*, 481, 898
- Lépine, S., et al. 2000, *AJ*, 120, 3201
- Mason, B. D., Gies, D. R., Hartkopf, W. I., Bagnuolo, W. G., Jr., ten Brummelaar, T., & McAlister, H. A. 1998, *AJ*, 115, 821
- Marchenko, S. V., Moffat, A. F. J., & Eenens, P. R. J. 1998, *PASP*, 110, 1416
- Moffat, A. F. J., Drissen, L., Lamontagne, R., & Robert, C. 1988, *ApJ*, 334, 1038
- Monnier, J. D., Tuthill, P. G., & Danchi, W. C. 1999, *ApJ*, 525, L97
- Monnier, J. D., Greenhill, L. J., Tuthill, P. G., & Danchi, W. C. 2002, *ApJ*, 566, 399
- Montes G., González R.F., Pérez-Torres M.A. & Alberdi A. (in preparation)
- Niemela, V. S. 1991, *Wolf-Rayet Stars and Interrelations with Other Massive Stars in Galaxies*, 143, 201
- Niemela, V. S., Gamen, R., Morrell, N. I., & Giménez Benítez, S. 1999, *Wolf-Rayet Phenomena in Massive Stars and Starburst Galaxies*, 193, 26
- Nugis, T., Crowther, P. A., & Willis, A. J. 1998, *A&A*, 333, 956
- Oskinova, L. M. 2005, *MNRAS*, 361, 679
- Panagia, N., & Felli, M. 1975, *A&A*, 39, 1
- Prinja, R. K., Stahl, O., Kaufer, A., Colley, S. R., Crowther, P. A., & Wolf, B. 2001, *A&A*, 367, 891
- Pittard, J. M., & Dougherty, S. M. 2006, *MNRAS*, 372, 801
- Pittard, J. M., Dougherty, S. M., Coker, R. F., O'Connor, E., & Bolingbroke, N. J. 2006, *A&A*, 446, 1001

- Pittard, J. M. 2009, arXiv:0908.1003
- Setia Gunawan, D. Y. A., Chapman, J. M., Stevens, I. R., Rauw, G., & Leitherer, C. 2003, A Massive Star Odyssey: From Main Sequence to Supernova, 212, 230
- Stevens, I. R. 1995, MNRAS, 277, 163
- Stevens, I. R., Blondin, J. M., & Pollock, A. M. T. 1992, ApJ, 386, 265
- Tuthill, P. G., Monnier, J. D., & Danchi, W. C. 1999, Nature, 398, 487
- Tuthill, P. G., Monnier, J. D., Lawrance, N., Danchi, W. C., Owocki, S. P., & Gayley, K. G. 2008, ApJ, 675, 698
- Underhill, A. B., & Hill, G. M. 1994, ApJ, 432, 770
- Usov, V. V. 1992, ApJ, 389, 635
- van der Hucht, K. A. 2001, New Astronomy Review, 45, 135
- Van Loo, 2005, Ph.D. Thesis, Royal Observatory of Belgium
- White, R. L. 1985, ApJ, 289, 698
- Williams, P. M., van der Hucht, K. A., Pollock, A. M. T., Florkowski, D. R., van der Woerd, H., & Wamsteker, W. M. 1990, MNRAS, 243, 662
- Williams, P. M., van der Hucht, K. A., & Spoelstra, T. A. T. 1994, A&A, 291, 805
- Williams, P. M., Dougherty, S. M., Davis, R. J., van der Hucht, K. A., Bode, M. F., & Setia Gunawan, D. Y. A. 1997, MNRAS, 289, 10
- Wright, A. E., & Barlow, M. J. 1975, MNRAS, 170, 41

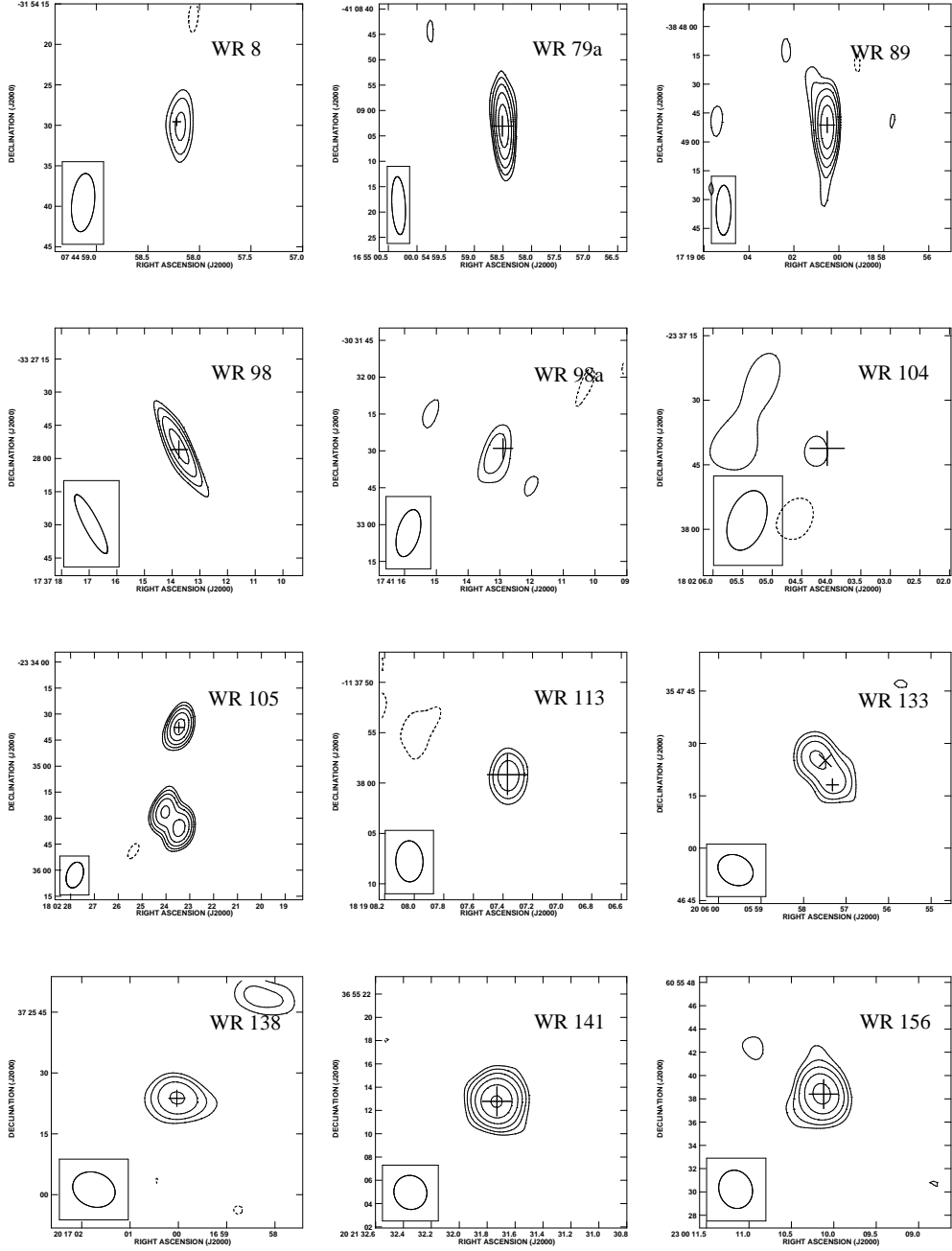


Fig. 1.— Contour image for the WR stars detected at 8.4 GHz of the 12 detected sources, including the tentative detection of WR 104. Contour lines are $-3, 3, 3\sqrt{3}, 9, \dots$ the rms noise. The rms noise is $\sim 50 \mu\text{Jy}$, except for WR 104 and WR 105 for which is ≈ 2 times higher, owing to their low declinations and the influence of extended sources within the field of view. The synthesized beam is drawn at the bottom left of each image. In each panel, the plus sing marks the optical positions of the star (we note that the size does not represent the uncertainty in the position). The cross-sign in the WR 133 image marks the peak of the emission at 4.8 GHz.

Table 1. Wolf Rayet Sample and their Properties

WR	Spectral Type	Binary Status	P (days)
8	WN7/WCE+?	SB1	38.4,115
12	WN8h+?	SB1,no d.e.l.	23.92
79a	WN9ha	VB	...
89	WN9h+OB	a.d.l.,VB	...
98	WN8/WC7	SB1	48.7
98a	WC8-9vd+?	CWB	565
104	WC9d+B0.5V	SB2,VB	243
105	WN9h
113	WC8d+O8-9IV	SB2	29.7
133	WN5+O9I	SB2,VB	112.4
138	WN5+B?	SB2,VB	11.6,1538
141	WN5+O5V-III	SB2	21.6
156	WN8h+OB?	d.e.l.	6.5,10

Note. — The values displayed in the columns were taken from the van der Hucht (2001) WR catalog.

Table 2. Calibrators

Source WR No.	Observation Date	Phase Calibrator	Bootstrapped flux (Jy) ^a				
			1.4 GHz	4.8 GHz	8.4 GHz	15 GHz	23 GHz
79a	07-Apr-21	1626-298	...	2.355±0.005	2.208±0.004
89	07-Apr-21	1626-298	...	2.355±0.005	2.208±0.004
98	07-Apr-21	1751-253	...	0.469±0.001	0.265±0.004
98a	07-Apr-21	1751-253	...	0.469±0.001	0.265±0.004
104	07-Apr-21	1820-254	...	0.630±0.005	0.695±0.002
105	07-Apr-21	1820-254	...	0.630±0.005	0.695±0.002
98	07-May-06	1744-312	...	0.570±0.005	0.637±0.003	...	0.590±0.006
133	07-May-06	2025+337	...	1.701±0.003	2.275±0.006	...	2.657±0.016
138	07-May-06	2025+337	...	1.701±0.003	2.275±0.006	...	2.657±0.016
8	08-Mar-07	0735-175	...	1.527±0.033	0.954±0.009	...	0.429±0.006
12	08-Mar-07	0735-175	...	1.527±0.033
79a	08-Mar-05	1626-298	...	2.759±0.030	2.696±0.008	...	1.952±0.044
113	08-Mar-05	1832-105	...	1.315±0.003	1.437±0.003	...	0.925±0.016
105	08-Mar-05	1820-254	...	0.932±0.019	0.877±0.016
141	08-Mar-08	2015+371	...	1.475±0.010	2.056±0.010	...	3.298±0.073
156	08-Mar-08	2148+611	...	1.360±0.003	1.068±0.004	...	0.714±0.016
105	99-Nov-20	1820-254	1.163±0.009	0.948±0.003	0.864±0.004
105	99-Nov-27	1820-254	...	0.953±0.002	...	0.778±0.0134	...
133	93-May-31	2005+403	2.60±0.03	3.14±0.05	3.12±0.08

Note. — ines separates the observing years.

^aThe bootstrapped fluxes and their uncertainties are those obtained from GETJY during the calibration.

Table 3. Radio Flux Densities and Spectral Indices

Source WR No.	Observation Date	Positions at 8.4 GHz (J.2000.0)			Fluxes (mJy)			α
		R.A.	Dec.	Error	4.8 GHz	8.4 GHz	23 GHz	
79a	07-Apr-21	16 54 58.51	-41 09 04.3	0.4	0.86±0.07	1.67±0.06	...	1.16±0.16
89	07-Apr-21	17 19 00.53	-38 48 52.0	0.2	1.82±0.24	3.01±0.08	...	0.88±0.24
98	07-May-06	17 37 13.82	-33 27 55.4	0.3	0.94±0.06	1.09±0.05	...	0.26±0.14
98a	07-May-06	17 41 13.12	-30 32 32.0	1.0	<0.39	0.59±0.06	...	>0.73
104 ^a	07-May-06	18 02 04.31	-23 37 41.4	0.8	<0.21	0.42±0.09	...	>1.22
105	07-May-06	18 02 23.44	-23 34 37.5	0.1	2.51±0.11	4.38±0.12	...	0.98±0.09
98	07-May-06	17 37 13.75	-33 27 54.9	0.4	0.58±0.06	1.18±0.05	1.94±0.15	0.64±0.07
133	07-May-06	20 05 57.25	+35 47 18.2	0.4	<0.41	0.31±0.03	0.57±0.07	0.60±0.15
138	07-May-06	20 17 00.01	+37 25 23.7	0.2	<0.12	0.52±0.03	1.15±0.08	>0.82
8	08-Mar-07	07 44 58.19	-31 54 30.0	0.3	0.22±0.04	0.28±0.03	0.30±0.05	0.17±0.15
12 ^a	08-Mar-07	08 44 47.18	-45 58 55.9	7.8	<0.22
79a	08-Mar-05	16 54 58.49	-41 09 03.0	0.1	0.99±0.04	1.56±0.05	2.31±0.14	0.54±0.05
105 ^b	08-Mar-05	18 02 23.46	-23 34 37.4	0.1	4.22±0.13	...	7.63±0.39	0.38±0.04
113	08-Mar-05	18 19 07.36	-11 37 59.3	0.1	0.22±0.03	0.47±0.04	1.27±0.07	1.06±0.09
141	08-Mar-08	20 21 31.73	+36 55 12.8	0.1	0.59±0.04	1.28±0.04	2.86±0.15	0.91±0.05
156	08-Mar-08	23 00 10.15	+60 55 38.4	0.1	0.77±0.04	0.99±0.04	1.59±0.09	0.46±0.05

Note. — Upper limits of the undetected sources were fixed as three times the rms noise of the map. For WR 133 at 4.8 GHz the upper limit was fixed from the peak of the unresolved emission. The α errors were estimated from, $\Delta\alpha^2 = [(\partial\alpha/\partial S_1)\Delta S_1]^2 + [(\partial\alpha/\partial S_2)\Delta S_2]^2$, for two frequency determinations of α , and from the error of the weighed linear regression fit used for the three frequency determinations. See Section 2 for details about the error of the flux densities determinations. Lines separate the observing epochs.

^aProbable detection. Coordinates refer to the local maximum position at 4.8 GHz for WR 12 and at 8.4 GHz for WR 104, both close to the optical positions.

^bPosition at 23 GHz.

Table 4. Radio Flux Densities and Spectral Index Comparison with Previous Observations

WR	$S_{1.4\text{ GHz}}$ (mJy)	$S_{2.4\text{ GHz}}$ (mJy)	$S_{4.8\text{ GHz}}$ (mJy)	$S_{8.4\text{ GHz}}$ (mJy)	$S_{15\text{ GHz}}$ (mJy)	$S_{23\text{ GHz}}$ (mJy)	α	Obs Date	Ref.	Spec. Type
8	0.36±0.03	01Nov12	CG04	
	0.22±0.04	0.25±0.03	...	0.30±0.05	0.17±0.15	08Mar05	TS	(T/NT) ^a
12	0.51±0.06	01Nov12	CG04	
	<0.22	08Mar05	TS	
79a	1.1±0.1	...	2.4±0.1	...	0.9±0.1	84Apr03	BA89	
	...	1.0±0.1	0.8±0.1	0.9±0.1	-0.1±0.1	Nov00	SC03	
	0.7±0.1	01Sep15	CG04	
	0.86±0.07	1.67±0.06	1.16±0.16	07Apr21	TS	
	0.99±0.04	1.56±0.05	...	2.31±0.14	0.54±0.05	08Mar05	TS	(T/NT) ^a
89	0.6±0.1	82Aug20	AB86	
	1.94±0.19	2.99±0.10	0.76±0.18	94Sep08	LC95	
	<1.20	<0.90	97Feb23	CL99	
	2.0±0.1	01Nov12	CG04	
	1.82±0.52	3.01±0.09	0.88±0.24	07Apr21	TS	(T) ^a
98	0.9±0.07	85Aug17	AB86	
	0.94±0.06	1.09±0.05	0.26±0.14	07Apr21	TS	
	0.58±0.06	1.18±0.05	...	1.94±0.15	0.64±0.07	07May06	TS	(T/NT?) ^c
98a	<0.36	...	0.37±0.07	0.60±0.05	0.64±0.11	0.57±0.10	0.30±0.22	00Feb24	MT02	
	0.47±0.05	01Oct08	CG04	
	<0.39	0.59±0.06	>0.73	07Apr21	TS	(T/NT) ^b
104	<0.4	84Apr04	AB86	
	<2.01	<0.39	94Sep07	LC97	
	<1.59	<0.99	97Feb23	CL99	
	<0.30	0.87±0.06	1.02±0.12	0.94±0.10	0.10± 0.23	00Feb25	MT02	
	0.54±0.06	01Nov12	CG04	
	<0.21	0.42±0.09	>1.22	07Apr21	TS	(T/NT) ^b
105	3.6±0.2	84Apr04	AB86	
	4.39±0.15	3.75±0.15	-0.28±0.01	94Sep07	LC97	
	<1.17	<0.69	97Feb23	CL99	
	1.43±0.20	...	2.92±0.08	4.77±0.10	0.81±0.04	99Nov20	TS	
	2.73±0.07	...	7.02±0.37	...	0.83±0.05	99Nov27	TS	
	5.4±0.1	01Nov12	CG04	
	2.51±0.11	4.38±0.12	0.98±0.09	07Apr21	TS	
	4.22±0.13	7.63±0.39	0.38±0.04	08Mar05	TS	(NT) ^a
113	≤0.4	80Jul26	BA82	
	<0.80	<0.80	94Sep07	LC97	
	<2.25	<0.90	97Feb23	CL99	
	0.75±0.04	01Nov12	CG04	

Table 4—Continued

	0.22 ± 0.03	0.47 ± 0.04	...	1.27 ± 0.07	1.06 ± 0.09	07May06	TS	(T) ^a
133	<0.3	85Aug17	AB86	
	<0.81	...	0.38 ± 0.08	0.27 ± 0.03	-0.65 ± 0.42	93May31	TS	
	0.36 ± 0.03	01Nov12	CG04	
	<0.41	0.31 ± 0.03	...	0.57 ± 0.07	0.60 ± 0.15	07May06	TS	(T/NT?) ^d
138	0.6 ± 0.1	80Jul27	BA82	
	<0.12	0.52 ± 0.03	...	1.15 ± 0.08	>0.82	07May06	TS	(T) ^a
141	0.6 ± 0.1	85Aug05	AB86	
	0.59 ± 0.04	1.28 ± 0.04	...	2.86 ± 0.15	0.91 ± 0.05	08Mar05	TS	(T) ^a
156	1.06 ± 0.03	01Nov12	CG04	
	0.77 ± 0.04	0.99 ± 0.04	...	1.59 ± 0.09	0.46 ± 0.05	08Mar05	TS	(T/NT) ^a

Note. — The whole frequency range observed was used for the spectral index and lower limits determinations, except for WR 133, for which the upper limits of the flux densities at the lower frequencies were not taken into account.

For all the sources spectral classification was done over the whole group of observations. (T) Thermal. (NT) Non-thermal. (T/NT) Composite, thermal+non-thermal. (T/NT?) tentative composite.

Spectral classification criteria used:

^aAccording to the criteria described in section 3.2.

^bStudy presented in MT02

^cAccording to the criteria described in section 3.2 and the short time variability ~ 15 days in the density flux.

^dAccording to the criteria described in section 3.2 and the flat tendency of the spectral index determination at the lower frequency range.

References. — TS:This Study; BA82: Bieging et al. (1982); BA89: Bieging et al. (1989); SC03: Setia Gunawan et al. (2003); MT02: Monnier et al. (2002).

Table 5. Mass-Loss Rate Determinations

WR	Spectral Type	v_{∞} (km s ⁻¹)	d (kpc)	μ	Z	γ	$S_{8.4 \text{ GHz}}$ (mJy)	$\dot{M}_{8.4 \text{ GHz}}$ 10 ⁻⁵ M _⊙ yr ⁻¹
8	WN7/WCE+?	1590	3.47	1.7	1.0	1.0	0.28	<1.79
79a	WN9ha	935	1.99	2.6	1.0	1.0	1.56	<2.67
89	WN9h+OB	1600	2.88	1.5	1.0	1.0	3.01	7.14
98	WN8/WC7	1200	1.9	3.7	1.0	1.0	1.09	<3.30
98a	WC8-9vd+?	2000	1.9	4.7	1.1	1.1	0.59	<4.03
104	WC9d+B0.5V	1220	2.3	4.7	1.1	1.1	0.42	<2.54
105	WN9h	700	1.58	2.6	1.0	1.0	4.38	<2.91
113	WC8d+O8-9IV	1700	1.79	4.7	1.1	1.1	0.47	2.64
133	WN5+O9I	1800	2.14	4.0	1.1	1.1	0.27	<2.06
138	WN5+B?	1400	1.26	4.0	1.1	1.1	0.52	1.18
141	WN5+O5V-III	1550	1.26	4.0	1.1	1.1	1.28	2.57
156	WN8h+OB?	660	3.56	3.3	1.0	1.1	0.99	<3.87

Note. — The logarithmic error in the \dot{M} estimates are 0.21 for the stars considered in cluster/association, and 0.41 for the rest (WR 98, 98a, 104 and 156).